Low-energy resonances in the $^{18}O(p, \gamma)^{19}F$ reaction

F. R. Pantaleo,[1,2,*] A. Boeltzig,[3,†] A. Best,[4,5] R. Perrino,[2,‡] M. Aliotta,[6] J. Balibrea-Correa,[4,5] F. Barile,[2] D. Bemmerer,[7] C. Broggini,[8] C. G. Bruno,[6] R. Buompane,[5,9] A. Caciolli,[8,10] F. Cavanna,[11,§] T. Chillery,[6] G. F. Ciani,[3] P. Corvisiero,[11,12] L. Csedreki,[3,13,14] T. Davinson,[6] R. J. deBoer,[15] R. Depalo,[8,10] G. D'Erasmo,[1,2] A. Di Leva,[4,5] Z. Elekes,[13] F. Ferraro,[11,12] E. M. Fiore,[1,2] A. Formicola,[3] Zs. Fülöp,[13] G. Gervino,[16,17] A. Guglielmetti,[18,19] C. Gustavino,[20] Gy. Gyürky,[13] G. Imbriani,[4,5] M. Junker,[3] I. Kochanek,[3] M. Lugaro,[21,22] E. Masha,[18] R. Menegazzo,[8] V. Mossa,[1,2] V. Paticchio,[2] D. Piatti,[8,10] P. Prati,[11,12] D. Rapagnani,[4,5] L. Schiavulli,[1,2] K. Stöckel,[7,23] O. Straniero,[3,24] T. Szücs,[13] M. P. Takács,[7,23,¶] D. Trezzi,[18,19] M. Wiescher,[15] and S. Zavatarelli[11]

(LUNA Collaboration)

[1]*Università degli Studi di Bari, Dipartimento Interateneo di Fisica, Via G. Amendola 173, 70126 Bari, Italy*
[2]*Istituto Nazionale di Fisica Nucleare, Sezione di Bari, Via E. Orabona 4, 70125 Bari, Italy*
[3]*Istituto Nazionale di Fisica Nucleare, Laboratori Nazionali del Gran Sasso (LNGS), Via G. Acitelli 22, 67100 Assergi, Italy*
[4]*Università degli Studi di Napoli "Federico II", Dipartimento di Fisica "E. Pancini", Via Cintia 21, 80126 Napoli, Italy*
[5]*Istituto Nazionale di Fisica Nucleare, Sezione di Napoli, Via Cintia 21, 80126 Napoli, Italy*
[6]*SUPA, School of Physics and Astronomy, University of Edinburgh, Peter Guthrie Tait Road, EH9 3FD Edinburgh, United Kingdom*
[7]*Helmholtz-Zentrum Dresden-Rossendorf, Bautzner Landstraße 400, 01328 Dresden, Germany*
[8]*Istituto Nazionale di Fisica Nucleare, Sezione di Padova, Via F. Marzolo 8, 35131 Padova, Italy*
[9]*Università degli Studi della Campania "L. Vanvitelli", Dipartimento di Matematica e Fisica, Viale Lincoln 5, 81100 Caserta, Italy*
[10]*Università degli Studi di Padova, Via F. Marzolo 8, 35131 Padova, Italy*
[11]*Istituto Nazionale di Fisica Nucleare, Sezione di Genova, Via Dodecaneso 33, 16146 Genova, Italy*
[12]*Università degli Studi di Genova, Via Dodecaneso 33, 16146 Genova, Italy*
[13]*Institute for Nuclear Research (Atomki), PO Box 51 H-4001 Debrecen, Hungary*
[14]*Gran Sasso Science Institute, Viale F. Crispi 7, 67100 L'Aquila, Italy*
[15]*The Joint Institute for Nuclear Astrophysics, Department of Physics, University of Notre Dame, Notre Dame, Indiana 46556, USA*
[16]*Università degli Studi di Torino, Via P. Giuria 1, 10125 Torino, Italy*
[17]*Istituto Nazionale di Fisica Nucleare, Sezione di Torino, Via P. Giuria 1, 10125 Torino, Italy*
[18]*Università degli Studi di Milano, Via G. Celoria 16, 20133 Milano, Italy*
[19]*Istituto Nazionale di Fisica Nucleare, Sezione di Milano, Via G. Celoria 16, 20133 Milano, Italy*
[20]*Istituto Nazionale di Fisica Nucleare, Sezione di Roma, Piazzale A. Moro 2, 00185 Roma, Italy*
[21]*Konkoly Observatory, Research Centre for Astronomy and Earth Sciences, Hungarian Academy of Sciences, 1121 Budapest, Hungary*
[22]*ELTE Eötvös Loránd University, Institute of Physics, Budapest 1117, Pázmány Péter sétány 1/A, Hungary*
[23]*Technische Universität Dresden, Institut für Kern- und Teilchenphysik, Zellescher Weg 19, 01069 Dresden, Germany*
[24]*INAF, Osservatorio Astronomico d'Abruzzo, Via Mentore Maggini, 64100 Teramo, Italy*

(Received 18 June 2020; revised 12 April 2021; accepted 6 July 2021; published 11 August 2021)

Background: Shell hydrogen burning during the asymptotic giant branch (AGB) phase through the oxygen isotopes has been indicated as a key process that is needed to understand the observed $^{18}O/^{16}O$ relative abundance in presolar grains and in stellar atmospheres. This ratio is strongly influenced by the relative strengths of the reactions $^{18}O(p, \alpha)^{15}N$ and $^{18}O(p, \gamma)^{19}F$ in low-mass AGB stars. While the former channel has been the focus of a large number of measurements, the (p, γ) reaction path has only recently received some attention and its stellar reaction rate over a wide temperature range rests on only one measurement.

Purpose: Our aim is the direct measurement of states in ^{19}F as populated through the reaction $^{18}O(p, \gamma)^{19}F$ to better determine their influence on the astrophysical reaction rate, and more generally to improve the understanding of the nuclear structure of ^{19}F.

*Corresponding author: francesca.pantaleo@ba.infn.it
†Corresponding author: axel.boeltzig@lngs.infn.it
‡Permanent address: Istituto Nazionale di Fisica Nucleare, Sezione di Lecce, via Arnesano, 73100, Lecce, Italy.
§Current address: Istituto Nazionale di Fisica Nucleare, Sezione di Torino, Via P. Giuria 1, 10125 Torino, Italy.
¶Current address: Physikalisch-Technische Bundesanstalt, Bundesallee 100, 38116 Braunschweig, Germany.

Method: Branchings and resonance strengths were measured in the proton energy range $E_p^{lab} = 150$–400 keV, using a high-purity germanium detector inside a massive lead shield. The measurement took place in the ultra-low-background environment of the Laboratory for Underground Nuclear Astrophysics (LUNA) experiment at the Gran Sasso National Laboratory, leading to a highly increased sensitivity.

Results: The uncertainty of the γ branchings and strengths was improved for all four resonances in the studied energy range; many new transitions were observed in the case of the 334 keV resonance, and individual γ decays of the 215 keV resonance were measured for the first time. In addition a number of transitions to intermediate states that decay through α emission were identified. The strengths of the observed resonances are generally in agreement with literature values.

Conclusions: Our measurements substantially confirm previous determinations of the relevant resonance strengths. Therefore the $^{18}O(p,\gamma)^{19}F$ reaction rate does not change with respect to the reaction rate reported in the compilations commonly adopted in the extant computations of red-giant branch and AGB stellar models. Nevertheless, our measurements definitely exclude a nonstandard scenario for the fluorine nucleosynthesis and a nuclear physics solution for the ^{18}O depletion observed in Group 2 oxygen-rich stardust grains.

DOI: 10.1103/PhysRevC.104.025802

I. INTRODUCTION

Observations of the oxygen isotopes, in particular in connection with the abundances of ^{15}N, ^{18}O, and ^{19}F in the atmosphere of red giant and asymptotic giant branch (AGB) stars can give insights into the interplay of mixing processes and nuclear burning operating in their interiors [1].

In addition, according to Nittler *et al.* [2] the $^{18}O/^{16}O$ ratio measured in stardust oxide grains, those belonging to the so-called Group 2, shows a substantial depletion of ^{18}O compared to the solar system value. The peculiar oxygen composition of these grains, which may form in the cool atmospheres of AGB stars, reflects the operation of deep mixing processes in stellar interiors [3,4].

The $^{18}O(p,\gamma)^{19}F$ reaction competes with the $^{18}O(p,\alpha)^{15}N$ reaction [5]. At the INFN Laboratori Nazionali del Gran Sasso (LNGS), the Laboratory for Underground Nuclear Astrophysics (LUNA) Collaboration has performed direct measurements of both reactions [5–7].

The effective background suppression in the Gran Sasso laboratory allowed for LUNA to measure the cross section of these reactions to proton energies as low as $E_p^{lab} = 60$ keV (p,α) and $E_p^{lab} = 90$ keV (p,γ). At these energies, only extrapolations from high-energy measurements were available before.

The reaction $^{18}O(p,\gamma)^{19}F$ ($Q = 7.994$ MeV) has a strong narrow resonance at $E_R^{lab} = 151$ keV (see Fig. 1), but a very low-energy (<100 keV) resonance [8] could influence the reaction rate. The strength of this resonance, however, is disputed [9,10]. A recent publication by the LUNA Collaboration presents the direct measurement of the $^{18}O(p,\gamma)^{19}F$ cross section between 160 and 90 keV [7].

Based on these measurements, the direct and resonant cross sections around 95 keV only have a minor impact on the stellar reaction rate in low-mass AGB stars.

The measurement reported by Best *et al.* [7] took advantage of a high efficiency bismuth germanium oxide (BGO) summing detector. The same detector was used to measure an excitation curve of $^{18}O(p,\gamma)^{19}F$ up to 400 keV, as shown in Sec. IV. The focus of the work presented here is the rich spectroscopic data provided by a high-purity germanium (HPGe) detector with its characteristic high energy resolution. Apart from the detector and the target holders, both data sets utilized the same experimental setup. The HPGe data set covers the energy range $E_p^{lab} = 150$–400 keV, including the high energy resonances up to the maximum energy ($E_p^{lab} = 400$ keV) afforded by the LUNA II accelerator.

Several measurements of environmental backgrounds were performed with both detector setups, and beam-induced background was investigated in the initial phase of the experiment, in order to understand the influence of the individual contaminants [11].

In this work we first describe the experimental setup, the target preparation, and discuss details of the target thickness monitoring through the yield measurement (Sec. II). In Sec. III we present and discuss the experimental method, the HPGe efficiency calibration, and sources of background. In Sec. IV we elaborate on the data for the measured resonances, namely at $E_R^{lab} = 151$, 215, 274, and 334 keV, with determination of branching ratios and resonance strengths. We report our conclusions in Sec. V.

II. EXPERIMENTAL SETUP AND TARGET PREPARATION

A. Accelerator and detectors

The proton beam for the present measurements was delivered on target by the LUNA II 400 kV electrostatic accelerator. It provided beam currents up to 300 μA with an energy spread of 0.1 keV in the energy range of $E_p^{lab} =$ 150–400 keV [12].

The target chamber was electrically isolated from the beamline and acted as a Faraday cup for measuring the accumulated charge. A cold finger, held at liquid nitrogen temperature, extended to less than 1 cm from the target surface and was biased to −300 V for secondary electron suppression.

The two phases of the experimental campaign correspond to different detector configurations: a 4π BGO detector surrounded the target chamber in the first phase [13], and an HPGe detector was placed at 55° with respect to the beam direction in the second phase.

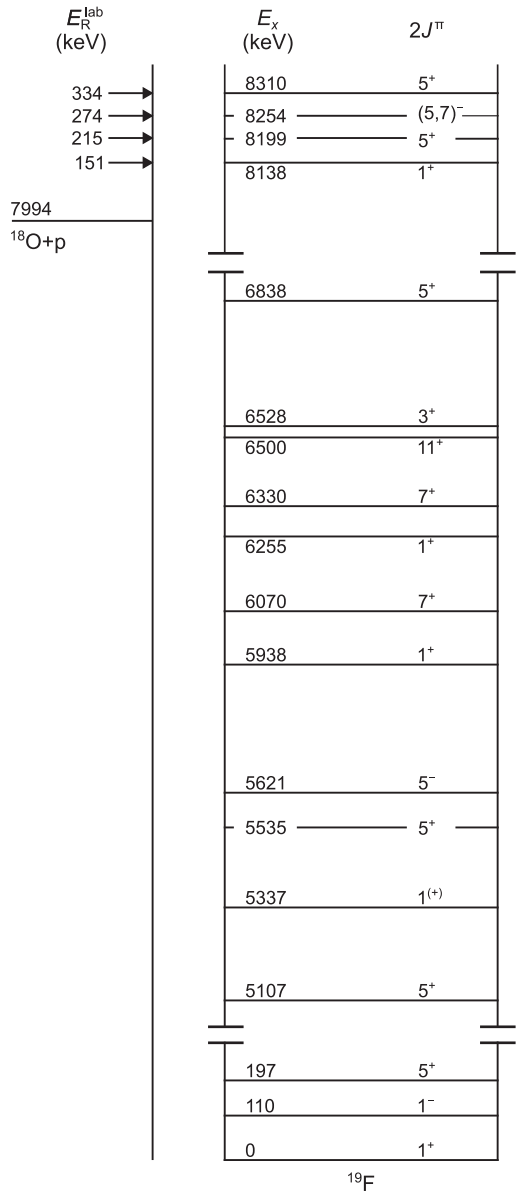

FIG. 1. Truncated ^{19}F level diagram (level information from [8]). The Q value for ^{18}O$(p,\gamma)^{19}$F is indicated ($Q = 7994$ keV), together with the states corresponding to the ^{18}O$(p,\gamma)^{19}$F resonances that are the subject of this work: at $E_R^{lab} = 151$, 215, 274, and 334 keV.

The detectors were shielded with a 10 cm and 15 cm thick layer of lead, respectively, in order to further reduce the environmental background [11,14,15]. Details of the beamline configuration are documented in Formicola *et al.* [12].

Here we discuss the HPGe phase of the experiment that utilized a coaxial HPGe detector (ORTEC) with a relative efficiency of 104%.

The detector was placed at an angle of 55° with respect to the beam axis to minimize angular distribution effects [16], and in a close geometry, at a distance of 20 mm from the beam spot on target. It was additionally shielded by 15 cm of lead (Fig. 2) to suppress backgrounds from environmental γ rays which were visible below 3 MeV.

FIG. 2. Lead shielding in the HPGe configuration. Left: close detector geometry (closed shielding); right: larger detector distance (open shielding).

B. Targets

The Ta_2O_5 targets were prepared by anodization [17] of 0.3 mm thin tantalum disks of 40 mm diameter. The isotopic enrichment was 99% in ^{18}O. These targets meet a number of specific requirements: uniform thickness, the ability to sustain a high beam current over an extended time, and a known and constant stoichiometry [18].

The tantalum disks were mechanically polished first and then cleaned in a citric acid solution for approximately one hour at a temperature of 90 °C. Citric acid was chosen instead of hydrofluoric acid to avoid contamination with fluorine that can give rise to an intense γ-ray background in the energy range of the experiment (see Sec. III B).

Voltages of 12 and 25 V were chosen for the anodization of the targets, corresponding to nominal thicknesses of the Ta_2O_5 layers (using Vermilyea's relation [18]) of about 25 and 50 nm, respectively. Over the energy range of the present measurement this corresponds to an energy loss of the projectile of 8 keV at the lowest energy and 6 keV at the highest energy for the thicker targets.

The high beam currents (up to 300 μA on target) induce a progressive deterioration of the effective target thickness and homogeneity, consequently modifying the reaction yield plateau [19].

To monitor this degradation in the present experiment, a resonance scan of the strong narrow resonance at $E_R^{lab} = 151$ keV was regularly performed (typically at least every 10 C). The stability of the target is illustrated with examples of measured resonance profiles in Fig. 3. Targets were replaced when changes in the back edge of the target profile became clearly visible, typically after an accumulated charge of about 20 to 25 C.

III. EXPERIMENTAL METHOD AND PROCEDURES

A. Efficiency determination

For large detection efficiencies (i.e., especially at small distances between detector and source), the effect of true coincidence summing on the detection efficiency has to be accounted for when measuring events emitting more than one γ ray in coincidence, e.g., as part of a a cascade [20]. The complexity of the necessary summing corrections increases with the number of the transitions in the decay scheme of the measured radionuclide. An easy case is ^{137}Cs: the dominant decay branch emits a single γ ray, consequently

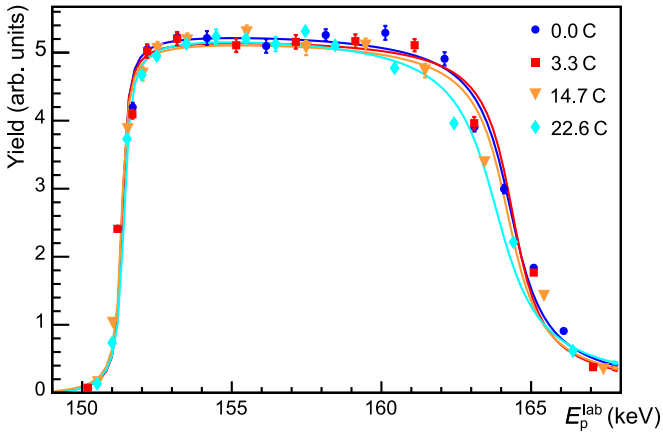

FIG. 3. Thick-target yield curve of the $E_R^{lab} = 151$ keV resonance illustrating the target thickness, and change of target profile with increasing accumulated charge. The fitted curves are shown to guide the eye.

measurements of ^{137}Cs are not affected by summing effects. In contrast, the decay of ^{60}Co and the ^{14}N$(p,\gamma)^{15}$O reaction produce γ-ray cascades, and are thus affected by summing. The γ decays of ^{60}Co and of ^{15}O through cascades involve at most one intermediate state, so that only the case of summing two coincident photons has to be considered. The corrections in this case are calculated as follows [21,22]:

$$\begin{aligned} N^{\mathrm{FEP}}(E_{\gamma_1}) &= AtB_{\gamma_1}\eta^{\mathrm{FEP}}(E_{\gamma_1})B_{\gamma_2}(1-\eta^{\mathrm{TOT}}(E_{\gamma_2})), \\ N^{\mathrm{FEP}}(E_{\gamma_2}) &= AtB_{\gamma_2}\eta^{\mathrm{FEP}}(E_{\gamma_2})B_{\gamma_1}(1-\eta^{\mathrm{TOT}}(E_{\gamma_1})), \\ N_{\mathrm{sum}}(E_{\gamma_1}+E_{\gamma_2}) &= AtB_{\gamma_1}B_{\gamma_2}\eta^{\mathrm{FEP}}(E_{\gamma_1})\eta^{\mathrm{FEP}}(E_{\gamma_2}), \end{aligned} \tag{1}$$

where N^{FEP} are the number of counts in the full-energy peaks, η^{FEP} and η^{TOT} are the full energy peak and total efficiencies, A is the γ-ray emission rate, B_{γ_i} is the branching ratio, and t is the live time of the measurement.

Thus, as in the example above, in a given detector-source geometry for each γ-ray with energy E_γ, two efficiencies have to be considered: the total efficiency η^{TOT}, that is the probability that the γ ray will deposit any amount of energy in the detector, and the full-energy peak efficiency η^{FEP}, that is the probability that all of energy E_γ is deposited in the detector. Typically, η^{FEP} is significantly smaller than η^{TOT}.

Empirical parametrizations [16,23] can be used to model η^{FEP} and η^{TOT} as functions of γ-ray energy and detector distance, whose parameters are to be determined by fitting the model to a set of calibration measurements. In this work, the efficiencies were parametrized as [24]

$$\eta^{\mathrm{FEP}}(d,E_\gamma) = f(d,E_\gamma)\times\exp\left(a+b\ln(E_\gamma)+c\ln(E_\gamma)^2\right) \tag{2}$$

and

$$\eta^{\mathrm{TOT}}(d,E_\gamma) = \frac{\eta^{\mathrm{FEP}}(d,E_\gamma)}{\exp\left(k_1+k_2\ln(E_\gamma)+k_3\ln(E_\gamma)^2\right)}, \tag{3}$$

where the function

$$f(d,E_\gamma) = \frac{1-\exp\left(\frac{d+d_0}{a_0+b_0\sqrt{E_\gamma}}\right)}{(d+d_0)^2} \tag{4}$$

models the change of efficiency with distance and a, b, c, k_1, k_2, k_3, d_0, b_0, a_0 are the fitting parameters. Their values were obtained through χ^2 minimization with respect to experimental data.

Experimental determinations of the HPGe detection efficiency were performed with ^{137}Cs and ^{60}Co calibration sources with known activities (relative uncertainty 1.5% at 95% confidence level) and extended to higher energies using the well known $E_R^{lab} = 278$ keV resonance in the ^{14}N$(p,\gamma)^{15}$O reaction ($Q = 7.297$ MeV).

The calibration measurements were performed at different distances, moving the detector on rails along the 55° axis. The closest geometry corresponds to an effective distance to the target surface (radioactive source or beam spot) of about 2 cm, but is referred to as detector position $d = 0$ cm in the following. Relative to this position, the additional distances used for calibration runs were $d = 5$, 10, and 15 cm.

The experimental data and the fit results are shown in Fig. 4. Correlations between the model parameters in the fit were not considered when propagating the systematic error of the efficiency curve. Instead, a systematic uncertainty of 4% was conservatively assumed over the γ-energy range covered by the parametrization (i.e., not including 110 and 197 keV) for the efficiency in close geometry.

For the $E_\gamma = 110$ and 197 keV γ rays, the efficiency changes rapidly as a function of energy, hindering a reliable extrapolation from higher energy data. Therefore, at these two energies a Monte Carlo simulation of the setup, based on GEANT4 [25], was used to obtain values for the detection efficiencies. From the simulation we obtained full-energy peak efficiencies of 4.51×10^{-3} and 4.51×10^{-2} and total efficiencies of 5.75×10^{-3} and 7.45×10^{-2}, for the 110 and 197 keV lines, respectively. Both energies correspond to secondary γ rays that contribute to summing effects, the systematic uncertainty of summing effects is discussed in Sec. IV E.

B. Beam-induced backgrounds

Beam-induced backgrounds can have a significant impact on the measurement of a reaction of interest. They are caused by reactions on impurities in or near the target and may influence or even dominate parts of the experimental spectra.

Resonances in the cross sections of the background reactions in the energy range of our ^{18}O$(p,\gamma)^{19}$F measurements may cause a particularly strong background contribution.

The radiative direct capture ^{12}C$(p,\gamma)^{13}$N reaction ($Q = 1.943$ MeV) has been observed in the HPGe spectra due to its nonresonant cross section.

The ^{19}F$(p,\alpha\gamma)^{16}$O reaction ($Q = 8.113$ MeV) is characterized by two resonances at proton energies of 224 and 340.5 keV, which result in the emission of three distinct γ rays at 6.13, 6.92, and 7.12 MeV [26,27] (the 6.13 MeV being dominant in the studied energy range). The background contribution from ^{19}F$(p,\alpha\gamma)^{16}$O is particularly critical for the ^{18}O$(p,\gamma)^{19}$F resonance measurements performed at 215 and 334 keV.

A strong resonance in the ^{23}Na$(p,\gamma)^{24}$Mg reaction ($Q = 11.693$ MeV) at $E_R^{lab} = 309$ keV sits close to the 334 keV resonance of the studied reaction.

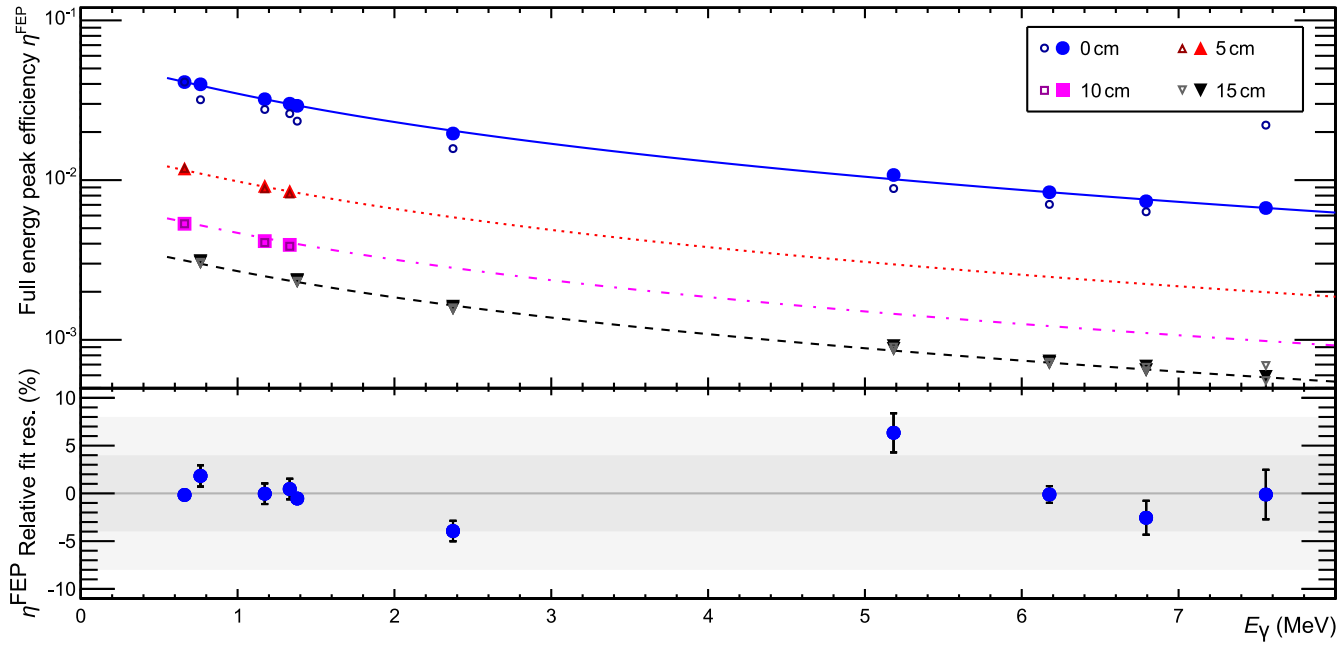

FIG. 4. Results of the efficiency calibration. Top panel: full-energy peak efficiency for a single γ ray as a function of energy and detector distance, with the lines for $d = 0$, 5, 10, 15 cm, plotted in order from top to bottom. The lines through the data points are the results from a fit. Open markers are efficiencies without corrections for summing effects, full markers include these corrections. Bottom panel: residuals at the detector distance of "0 cm"; the shaded bands indicate the relative uncertainty assigned to the efficiency (the inner band corresponds to the assigned 4.0%, the outer band to twice that value).

Lastly, a resonance at 278 keV in ^{14}N$(p,\gamma)^{15}$O ($Q =$ 7.556 MeV) is very close in energy to the 274 keV resonance of ^{18}O$(p,\gamma)^{19}$F.

Backgrounds from these reactions were identified in the spectra, and subtracted for our final analysis.

IV. DATA ANALYSIS AND RESULTS

The data taking focused on scans and measurements of the resonances at $E_R^{lab} = 151$, 215, 274, and 334 keV, as discussed in the following Secs. IV A, IV B, IV C, and IV D, respectively. The calculation of branching ratios for the individual resonances is presented in Sec. IV E, and the resulting resonance strengths are discussed in Sec. IV F. The astrophysical reaction rate resulting from our measured resonance properties is discussed in Sec. IV G. Additional data points were acquired between these resonances, covering the energy range of $E_p^{lab} = 150$–400 keV, to study for beam-induced backgrounds.

The excitation function from BGO measurements is shown in Fig. 5. A detailed analysis of the low-energy region below 100 keV, that is not shown here, is given in Best *et al.* [7].

All measurements were performed with the detector in close geometry to the target. We began the data analysis by identifying all transitions between states in the compound nucleus and assigning them to cascades. Peak areas were determined, accounting for possible sources of background. Then we derived branching ratios and the resonance strengths.

A. 151 keV resonance

The resonance at $E_R^{lab} = 151$ keV, being the strongest and best known resonance of the ^{18}O$(p,\gamma)^{19}$F reaction, was regularly scanned for each target to check and monitor the target degradation during the long beam irradiation. Spectra from several runs (152.4 keV $\leqslant E_p \leqslant$ 168.1 keV) were summed to enhance weak primary transitions from the resonant state at $E_x = 8138$ keV. We could identify all transitions known from the literature [28], plus a transition to the 5337 keV state which has not been observed previously. The yield of the newly observed transition, compared to the yield of the well-established transition to $E_f = 3908$ keV, is shown for a scan of the $E_R^{lab} = 151$ keV resonance in Fig. 6.

The eight primary transitions are indicated in the spectrum in Fig. 7. Escape and double escape peaks of the reaction of interest were also identified.

The primary peak at $E_\gamma = 2200$ keV overlaps with an environmental background line from ^{214}Bi, which had to be subtracted based on the measured environmental background rate.

For the three primary transitions to states at $E_f = 6255$, 5938, and 5337 keV, no secondary γ rays are visible in the spectra.

For the $E_f = 5938$ and 6255 keV we have to take into account [29] that the γ decay competes with α-particle emission (leaving ^{15}N as a residual). According to [30,31], the α channel is dominant in the decay of the state at 5938 keV. For the 6255 keV state, α-particle emission is the only observed decay [8], as also confirmed by the lack of $\gamma\gamma$ coincidences

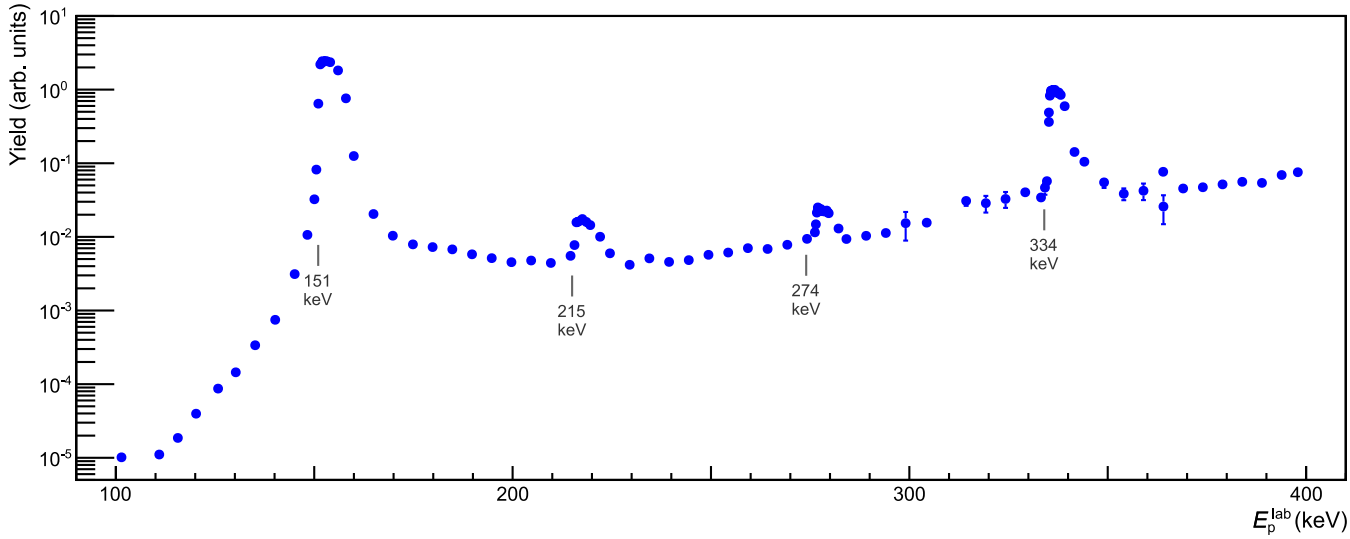

FIG. 5. Excitation function from the BGO measurements. The measurements include direct capture range and the high energy resonances at 151, 215, 274, and 334 keV.

when the level is fed from the 8138 → 6255 keV primary transition [32].

Similarly, for the 5337 keV level is reported [31] to predominantly α decay. The γ-decay channel of this level is present [8], but its branching ratio is too small to be detected in our experiment. The five other observed primary transitions (final states $E_f < 4$ MeV) have a clear signature with all secondary γ rays [8] visible in the spectrum.

B. 215 keV resonance

The strength of the resonance at $E_R^{lab} = 215$ keV was known from previous works [28,33,34].

In the present work we analyzed two spectra taken at $E_p = 223.8$ keV and determined the branching ratios of the associated primary transitions for the first time.

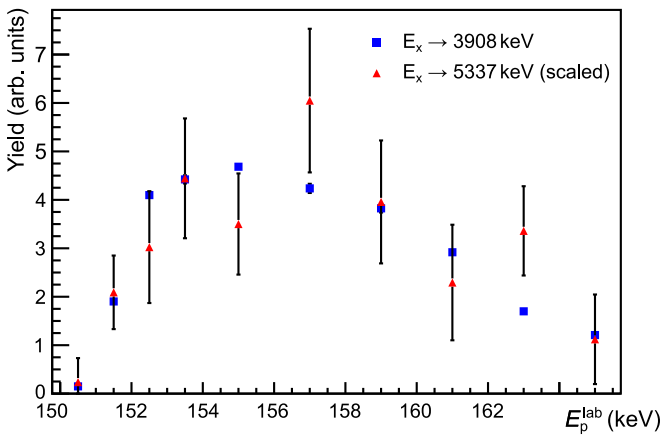

FIG. 6. Yields of the well-known transition to $E_f = 3908$ keV and the newly observed transition to $E_f = 5337$ keV when scanning over the $E_R^{lab} = 151$ keV resonance. Yields have been scaled relative to each other for this visualization.

Seven primary transitions and the corresponding secondary transitions were seen; the primary transitions are marked in the spectrum in Fig. 8.

Besides the peaks from the reaction of interest, background peaks from the $^{19}F(p,\alpha\gamma)^{16}O$ reaction are present, but the energies of contaminant and environmental background peaks do not overlap with the energies of the primaries. As in the case of the 151 keV resonance, a primary γ ray for the transition to $E_f = 5535$ keV was observed, without detecting any secondary γ-rays associated with the decay of this level. All other states ($E_f < 4$ MeV) observed in primary transitions are also visible through the secondary γ rays [8] present in the spectrum.

C. 274 keV resonance

The resonance at $E_R^{lab} = 274$ keV was studied analyzing a spectrum taken at $E_p = 279.5$ keV (shown in Fig. 9). Seven primary transitions were identified in this spectrum, starting from the resonant state at $E_x = 8254$ keV. All excited states involved have $E_f < 4$ MeV, with the γ channel dominant over the α channel [8], so that the secondary transitions are visible in the spectrum. Compared to previous works [28], three new primary transitions were detected. In this energy range, we observed contaminant peaks coming from the $^{14}N(p,\gamma)^{15}O$ reaction, with its nearby resonance at $E_R^{lab} = 278$ keV [24].

In particular, a primary at $E_\gamma = 6795$ keV overlaps with the $^{14}N(p,\gamma)^{15}O$ peak at 6797 keV. This background peak was subtracted, using the spectrum acquired with $^{14}N(p,\gamma)^{15}O$ on resonance during the efficiency calibration.

D. 334 keV resonance

The highest $^{18}O(p,\gamma)^{19}F$ resonance accessible at the LUNA II accelerator was studied by analyzing a spectrum acquired at $E_p = 340.0$ keV (Fig. 10). Eighteen primary transitions from the resonant state at $E_x = 8310$ keV were

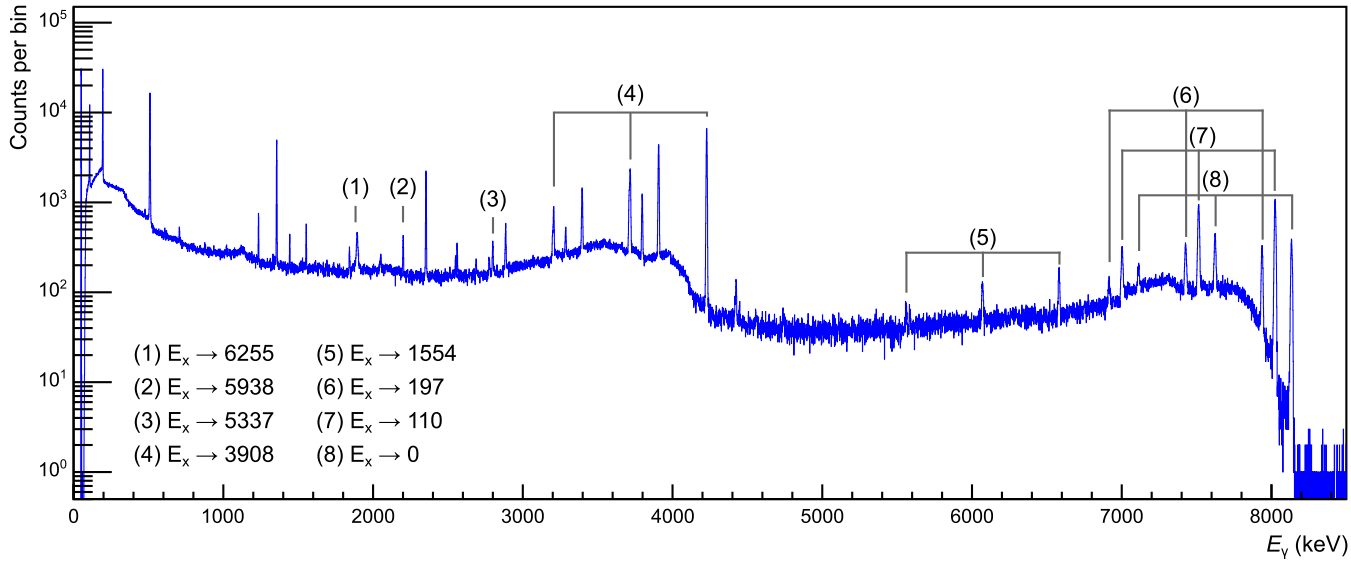

FIG. 7. HPGe spectrum acquired on the 151 keV resonance, with all observed primary transitions indicated.

identified in this spectrum. Two weak peaks with energies that could hint at previously unobserved primary transitions to levels at 6838 and 5107 keV but were not included in the calculation of resonance strength and branching ratio, due to their large statistical uncertainties.

Among the sixteen primary transitions detected, thirteen are new, compared to Wiescher *et al.* [28]. The states below $E_f = 5$ MeV were all observed to decay through γ-ray cascades [8]. For the remaining states ($E_f > 5$ MeV), no secondary γ-ray cascades were observed and the same considerations discussed previously regarding the open α channels [31,35,36] apply.

Contaminant peaks coming from the $^{19}\mathrm{F}(p,\alpha\gamma)^{16}\mathrm{O}$, $^{23}\mathrm{Na}(p,\gamma)^{24}\mathrm{Mg}$, and $^{12}\mathrm{C}(p,\gamma)^{13}\mathrm{N}$ reactions were identified in the spectrum. Owing to a resonance at $E_R^{lab} = 340.5$ keV, the $^{19}\mathrm{F}(p,\alpha\gamma)^{16}\mathrm{O}$ reaction creates a strong background in this spectrum. Background from the $E_R^{lab} = 309$ keV resonance in $^{23}\mathrm{Na}(p,\gamma)^{24}\mathrm{Mg}$ is also visible [37], but its peaks do not overlap those of the studied reaction.

Peaks of the strongest $E_R^{lab} = 151$ keV resonance are seen in the spectrum, due to weak contribution from oxygen contaminants deep in the target (at a projectile energy of 151 keV). These primary peaks do not overlap with the peaks of the resonance at 334 keV.

E. Branching ratios calculation and results

For each studied resonance, we determined the number of counts for the γ-ray lines corresponding to the primary transitions for all experimental spectra. Starting from these experimental quantities, we determined the branching ratios, using the energy-dependent efficiency as described in Sec. III.

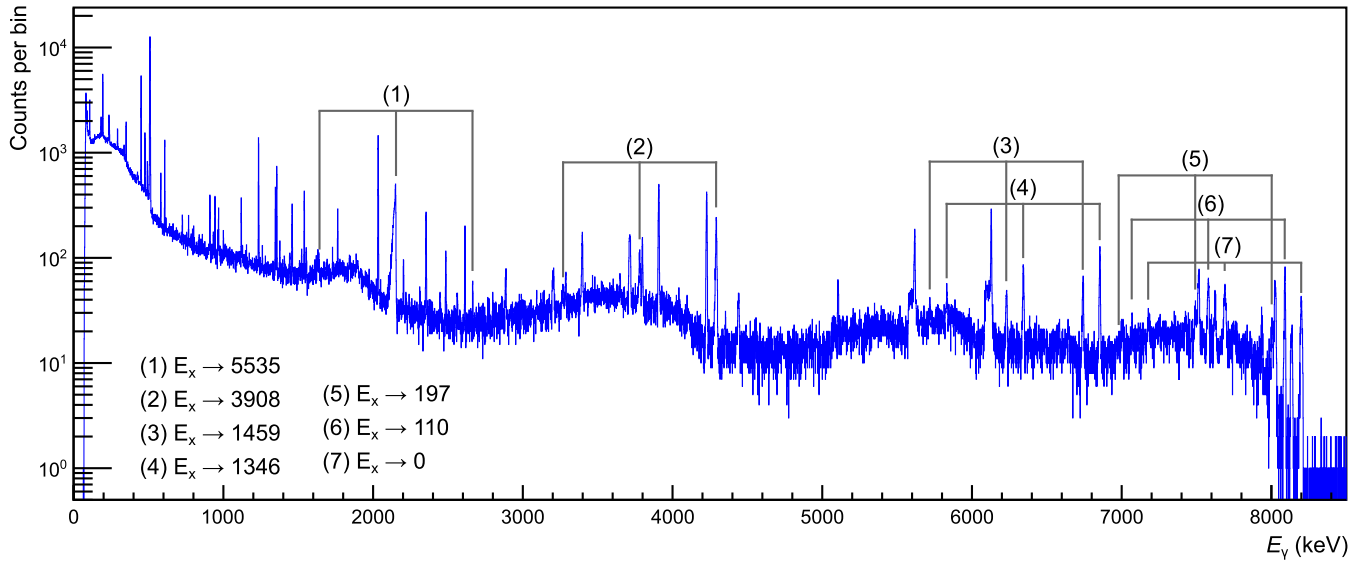

FIG. 8. HPGe spectrum acquired on the 215 keV resonance, with all observed primary transitions indicated.

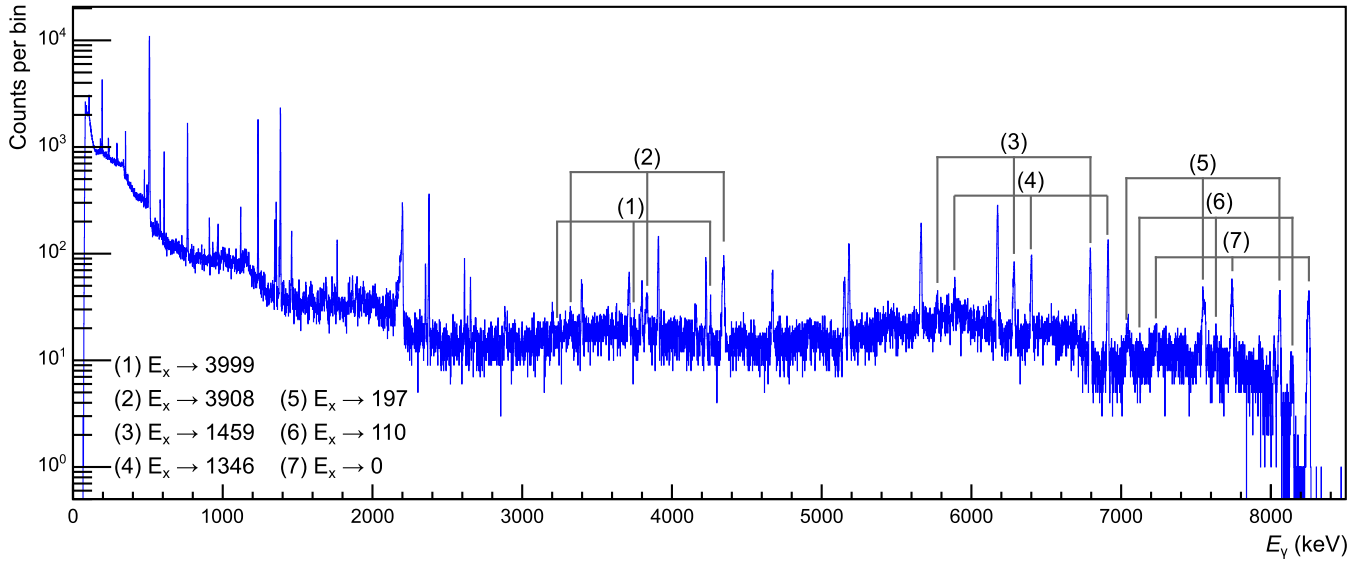

FIG. 9. HPGe spectrum acquired on the 274 keV resonance, with all observed primary transitions indicated.

To account for summing corrections, we used the calibrated efficiencies η^{FEP} and η^{TOT} to calculate the probabilities of each possible primary transition to either contribute to the full-energy peak corresponding to its own energy, or to contribute to the full energy peak of other primary transitions with larger energies (via summing-in). Branching ratios for secondary transitions for the calculation were taken from Tilley *et al.* [8].

Following the notation in [21,22], the probability P_E that a decay of a given nucleus registers as a count in the full energy peak at the energy E may be written as [21,22]

$$P_E = \sum_C \left[\prod_{m=1}^{M_C} \left(B_m \, \eta_m^{\mathrm{FEP}} \right) \prod_{n=M_C+1}^{N_C} B_n \left(1 - \eta_n^{\mathrm{TOT}} \right) \right], \quad (5)$$

which includes the sum over all cascades C, with N_C as the number of level transitions in the cascade C. M_C is the number of photons contributing to the full energy peak ($\sum_{m=1}^{M_C} E_m = E$), and $N_C - M_C$ are the photons that are not detected. B_i denotes the branching ratio of transition i. η_m^{FEP} and η_n^{TOT} are the full energy and the total efficiencies at E_m and E_n, respectively.

In our calculation, all probability values are then arranged in a matrix $\{P_{ij}\}$, with their elements representing the probability that the primary transition with index j contributes to the full energy peak of primary transition i, i.e., P_{ij} is calculated as P_{E_i} in Eq. (5), but with the sum limited to cascades C that include the primary transition j. Finally, the number N_i/N_R of counts per number of reactions in each primary peak is used

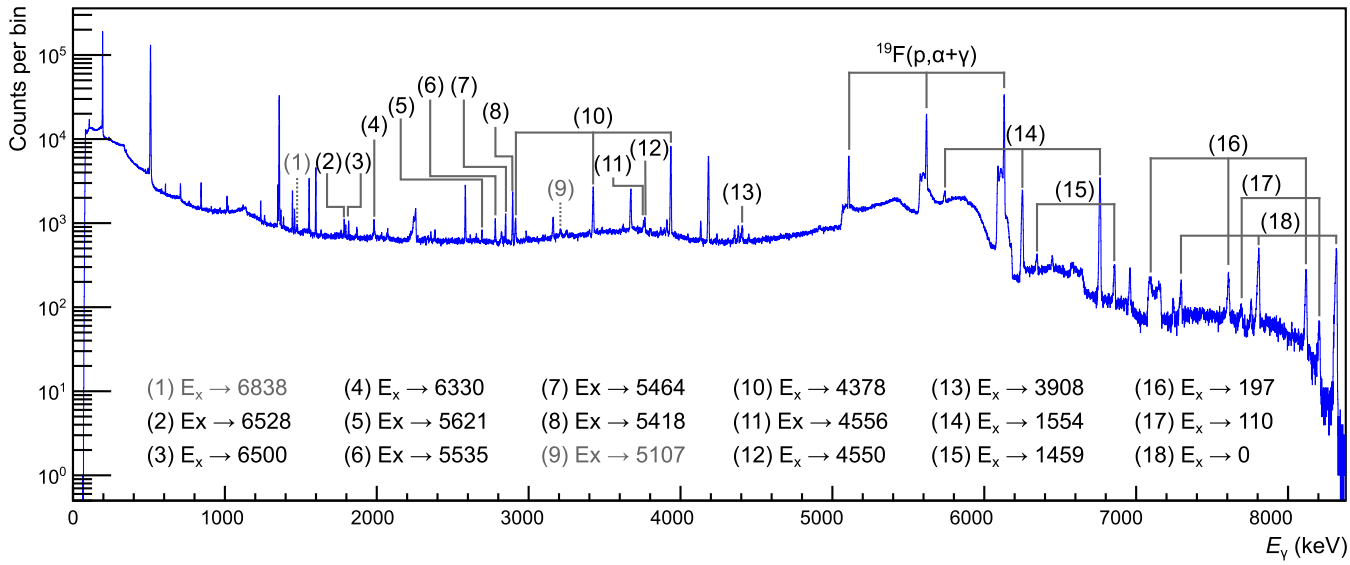

FIG. 10. HPGe spectrum acquired on the 334 keV resonance, with primary transitions (black) and hints for possible primary transitions (gray) indicated.

TABLE I. Primary branching ratios of the 151 keV resonance, corresponding to the $E_x = 8138$ keV state. The intermediate states in bold font were not observed to γ-decay to the ground state.

		Branchings (%)			
		This work	Wiescher	Dermigny *et al.* [32]	
E_γ (keV)	E_f (keV)	(stat.) (syst.)	*et al.* [28]	Singles	$\gamma\gamma$ coinc.
1883	**6255**	**1.49 ± 0.34 ± 0.12**	**3 ± 1**	**1.4 ± 0.2**	
2200	**5938**	**0.76 ± 0.28 ± 0.07**	**1.0 ± 0.5**	**0.9 ± 0.2**	<1.3
2800	**5337**	**0.73 ± 0.28 ± 0.06**			
4230	3908	55.4 ± 2.3 ± 3.9	54 ± 2	57.4 ± 0.5	58.0 ± 0.6
6583	1554	2.1 ± 0.8 ± 0.2	2 ± 1	1.2 ± 0.2	1.0 ± 0.2
7941	197	6.3 ± 0.6 ± 0.5	8 ± 1	7.1 ± 0.5	7.9 ± 0.9
8028	110	24.1 ± 0.3 ± 2.0	24 ± 2	23.5 ± 0.6	24.7 ± 1.0
8138	0	9.1 ± 0.3 ± 0.8	8 ± 2	8.5 ± 0.5	6.8 ± 0.8

to complete a system of linear equations, with the branching ratios B_i of the primary transition as unknown quantities:

$$\begin{pmatrix} N_1 \\ N_2 \\ \cdot \\ \cdot \\ N_n \end{pmatrix} = N_R \begin{pmatrix} P_{11} & \cdots & P_{1n} \\ P_{21} & \cdots & P_{2n} \\ \cdot & \cdots & \cdot \\ \cdot & \cdots & \cdot \\ P_{n1} & \cdots & P_{nn} \end{pmatrix} \begin{pmatrix} B_1 \\ B_2 \\ \cdot \\ \cdot \\ B_n \end{pmatrix}, \tag{6}$$

with the normalization condition on branching ratios

$$\sum_i B_i = 100\%. \tag{7}$$

Equation (5) does not account for anisotropic emission of the γ rays. Whilst the detector position at 55° minimizes susceptibility to angular distributions of the primary γ rays, angular correlations between γ rays in a cascade may affect the probabilities for summing to occur. For the case of ^{14}N$(p,\gamma)^{15}$O we conducted two Monte Carlo simulations: one for isotropic emission of all secondary γ rays, and one with angular correlations following [38]. Differences in all lines but the direct capture to the ground state were smaller than 0.5% (relative) between the two simulations. The ground state transition in ^{14}N$(p,\gamma)^{15}$O is a special case, as the ground state is weak and dominated by summing in for large detection efficiencies. The correction owing to angular correlations amounts to 4% for this line. For ^{18}O$(p,\gamma)^{19}$F, summing corrections were generally small, and as such angular correlations were not considered in the summing corrections.

Regarding the two low-energy γ lines for which the efficiency was determined through the Monte Carlo simulation, the summing-out contribution from the 110 keV line is practically negligible (due to the small total efficiency). Summing out caused by the 197 keV line can be appreciable, however. This is particularly true for the primary transition to the $E_f = 197$ keV state, for which the summing-out correction directly depends on $\eta^{\mathrm{TOT}}(197\ \mathrm{keV})$. We conservatively assume a systematic uncertainty of 50% on the summing correction to include the neglected angular correlations, uncertainties of the branching ratios for the secondary transitions, and the uncertainty in detection efficiency for the 110 and 197 keV γ rays taken from a Monte Carlo simulation.

The resulting primary branching ratios and their uncertainties for each of the four resonances are reported and compared to literature values in Tables I–IV.

Table I lists the primary branching ratios obtained for the 151 keV resonance. Since the newly detected primary at 2800 keV has a branching ratio of less than 1%, all other branching ratios are in fair agreement with the literature values.

Table II shows the primary branching ratios obtained for the 215 keV resonance, which were measured here for the first time.

Table III presents the primary branching ratios obtained for the 274 keV resonance. There are three new primary transitions compared to the literature values. The primary branching ratio regarding the 8254 → 1459 keV transition is significantly smaller than the value reported in literature. The literature value might be affected by a background contribution from ^{14}N$(p,\gamma)^{15}$O (see the discussion in Sec. IV C).

Table IV shows the primary branching ratios obtained for the 334 keV resonance. There are thirteen new primary branching ratios compared to the literature values. The intensity of these thirteen primary transitions is low, in fact the majority are characterized by branching ratios lower than 1%. The three primary branching ratios that are in common with the literature values are consequently lower, because of the

TABLE II. Primary branching ratios of the 215 keV resonance, corresponding to the $E_x = 8199$ keV state. The intermediate state in bold font was not observed to γ decay to the ground state.

		Branchings (%)
E_γ(keV)	E_f (keV)	This work ± (stat.) ± (syst.)
2664	**5535**	**1.46 ± 0.32 ± 0.11**
4291	3908	31.8 ± 2.3 ± 2.1
6740	1459	10.7 ± 0.7 ± 0.4
6853	1346	20.1 ± 0.5 ± 0.9
8002	197	8.4 ± 1.9 ± 0.5
8089	110	14.4 ± 0.2 ± 1.0
8199	0	13.1 ± 0.2 ± 1.0

TABLE III. Primary branching ratios of the 274 keV resonance, corresponding to the $E_x = 8254$ keV state.

		Branchings (%)	
E_γ(keV)	E_f (keV)	This work ± (stat.) ± (syst.)	Wiescher *et al.* [28]
4257	3999	2.9 ± 0.9 ± 0.3	
4346	3908	14.4 ± 2.8 ± 2.0	25 ± 8
6795	1459	5.6 ± 0.2 ± 0.2	24 ± 8
6910	1346	35.0 ± 2.4 ± 1.6	33 ± 10
8057	197	14.1 ± 0.4 ± 1.1	18 ± 7
8144	110	3.77 ± 0.07 ± 0.34	
8254	0	24.2 ± 1.6 ± 1.9	

strength fragmentation detected in the present high resolution measurement.

F. Resonance strengths

The experimental observable to calculate the resonance strength is the yield Y on the resonance plateau. In this analysis we already determined the resonance yield and its statistical uncertainty as part of the branching ratio calculation [N_R in Eq. (6)]. The value of the strength is then calculated as $\omega\gamma = 2\,\varepsilon_{\rm eff}(E_{\rm R})\,Y/\lambda^2$, where $\varepsilon_{\rm eff}(E_{\rm R})$ is the effective stopping power at the resonance energy, λ^2 is equal to $\frac{2\pi\hbar}{2\mu E_{\rm res}}$, μ is the reduced mass of the two-particle system, and $\hbar$ is the reduced Planck constant.

For protons in solid Ta_2O_5 with an isotopic enrichment in ^{18}O of 99%, the effective stopping power in the center-of-mass system is [19]

$$\varepsilon_{\rm eff} = \frac{M_{^{18}\rm O}}{M_{\rm p} + M_{^{18}\rm O}} \frac{N_{\rm O}}{N_{^{18}\rm O}} \left(\varepsilon_{^{18}\rm O} + \frac{N_{\rm Ta}}{N_{\rm O}} \varepsilon_{\rm Ta}\right). \tag{8}$$

TABLE IV. Primary branching ratios of the 334 keV resonance, corresponding to the $E_x = 8310$ keV state. The intermediate states in bold font were not observed to γ decay to the ground state.

		Branchings (%)	
E_γ (keV)	E_f (keV)	This work ± (stat.) ± (syst.)	Wiescher *et al.* [28]
1782	**6528**	**0.69 ± 0.09 ± 0.08**	
1810	**6500**	**0.58 ± 0.12 ± 0.06**	
1980	**6330**	**0.95 ± 0.12 ± 0.10**	
2689	**5621**	**0.41 ± 0.11 ± 0.04**	
2775	**5535**	**0.99 ± 0.10 ± 0.11**	
2846	**5464**	**1.50 ± 0.10 ± 0.16**	
2892	**5418**	**3.58 ± 0.04 ± 0.39**	
3754	4556	0.96 ± 0.30 ± 0.05	
3760	4550	1.16 ± 0.22 ± 0.05	
3932	4378	34.05 ± 0.85 ± 1.70	40 ± 2
4402	3908	1.13 ± 0.15 ± 0.08	
6756	1554	40.73 ± 0.98 ± 1.99	48 ± 2
6851	1459	2.60 ± 0.22 ± 0.11	
8113	197	3.13 ± 0.14 ± 0.38	
8200	110	0.76 ± 0.12 ± 0.10	
8310	0	6.78 ± 0.05 ± 0.74	12 ± 1

In the particular case

$$\varepsilon_{\rm eff} = \frac{18}{19} \frac{1}{0.99} \left(\varepsilon_{^{18}\rm O} + \frac{2}{5}\,\varepsilon_{\rm Ta}\right), \tag{9}$$

with the masses in amu, $\varepsilon_{^{18}\rm O}$, $\varepsilon_{\rm Ta}$ as the laboratory stopping powers of protons in units of eV cm^2/atom, calculated with the software SRIM-2013 [40], and N_i are number densities ($N_{\rm O} = N_{^{16}\rm O} + N_{^{17}\rm O} + N_{^{18}\rm O}$).

In addition to the previously discussed systematic uncertainties of efficiency and summing corrections, further systematic uncertainties contributed to the calculation of the resonance strengths. These contributions included the beam current reading (2.5%), resonance energies (below 1% except for $E_{\rm R}^{\rm lab} = 274$ keV), and effective stopping power. The uncertainty of the stopping power was evaluated from the mean stopping power errors in the 89–400 keV energy range for tantalum and oxygen equal to 5.8% and 2.9%, respectively [40]. An uncertainty of 5% was considered for the stoichiometry of the targets [17]. Combining these uncertainties in quadrature according to Eq. (9), we arrive at a systematic uncertainty of the effective stopping power of 4.5%.

The resonance strengths determined in the present experiment are reported in Table V. The results from the HPGe measurements are generally in agreement with the literature values.

G. Astrophysical reaction rate

In view of the reaction rate we confirm the current scenario [10,28,41]. For $0.02 < T_9 < 0.06$, the rate is dominated by the direct capture component and by the long tail of the 151 keV resonance. A very weak contribution, peaked at $T_9 \approx 0.05$, is due to the 95 keV resonance. Note that, according to our direct measurements [7], the strength of this resonance is in agreement with the upper limit determined in Ref. [32] and orders of magnitude smaller than the value obtained by [10] on the basis of an indirect search. Above $T_9 = 0.06$, the reaction rate is dominated by the 151 keV resonance, for which we obtain a strength in substantial agreement with previous findings [7,28,32–34,39]. The other resonances studied in the present paper are too narrow to contribute to the rate at the relevant astrophysical temperature. In addition we confirm the literature strength of the $E_{\rm p} = 334$ keV resonance, which is used as standard for the strengths of 14 other higher-energy resonances between 664 keV and 2 MeV [28]. As a result, in the temperature range $0.02 < T_9 < 0.15$, our new rate is in good agreement with those reported in the NACRE database [41] and in the STARLIB repository [34], except for $T_9 \approx 0.05$, where our rate is about a factor of 4 smaller that the one by NACRE. This discrepancy is probably due to the higher value assumed by [41] for the 95 keV resonance strength.

As a whole, our finding does not affect the stellar nucleosynthesis predictions for the ^{18}O/^{16}O ratio measured in stardust oxide grains and in the photosphere of red giant and AGB stars. In particular, based on the present study and [6], we can exclude a nuclear physic solution for the observed ^{18}O depletion shown by Group 2 stardust grains. Similarly, our

TABLE V. Resonance strengths obtained in this work, compared to literature values.

	$\omega\gamma$							
E_R^{lab} (keV)	This work (stat.) (syst.)	Best *et al.* [7]	Wiescher *et al.* [28]	Vogelaar *et al.* [33]	Iliadis *et al.* [34]	Dermigny *et al.* [32]	Becker *et al.* [39]	
151	$1.05 \pm 0.03 \pm 0.09$	0.88 ± 0.07	1.0 ± 0.1	0.92 ± 0.06		1.05 ± 0.08	1.1 ± 0.1	meV
215	$8.0 \pm 0.3 \pm 0.7$		>8	5 ± 1	5 ± 1			μeV
274	$31 \pm 1 \pm 3$		37 ± 5		24 ± 5			μeV
334	$0.95 \pm 0.01 \pm 0.10$		0.95 ± 0.08					meV

new reaction rate marginally affects the predictions of fluorine production by AGB stars [42].

V. CONCLUSIONS

We presented new measurements aimed at a more accurate characterization of the low-energy resonances in $^{18}O(p,\gamma)^{19}F$. The very low-background environment of the LNGS allowed a detailed investigation of the low-energy excitation function [7].

In total we studied four resonances at $E_p^{lab} = 151, 215, 274,$ and 334 keV.

Due to the excellent energy resolution of the HPGe detector and the low-background environment, an accurate treatment of the complex coincidence summing corrections was possible. This allowed us to measure the branching ratios of the 215 keV resonance, not previously available in literature, and provide an improved determination of the branching ratios for the resonances at $E_R^{lab} = 151, 274,$ and 334 keV.

For the 274 keV resonance we observed γ rays of three new primary transitions, which were not reported in the literature, and one branching ratio that deviates from the literature value, after subtraction of a background from $^{14}N(p,\gamma)^{15}O$.

Thirteen new γ-ray primaries were observed for the 334 keV resonance. Branching ratios of the stronger transitions are generally in agreement with literature values.

In summary, we have improved the experimental knowledge of the reaction $^{18}O(p,\gamma)^{19}F$, in particular of the primary branching ratios and strengths for resonances below 400 keV. We observed a number of new transitions for states in the ^{19}F compound nucleus, populated in $^{18}O(p,\gamma)^{19}F$, in particular for the previously poorly known decay of the resonance at 215 keV. Our findings confirm the current scenario for the astrophysical reaction rate for this reaction.

ACKNOWLEDGMENTS

D. Ciccotti and the technical staff of the LNGS are gratefully acknowledged for their help. This work was supported by the INFN. Following authors acknowledge funding: C.G.B., T.C., T.D., and M.A. via the STFC UK (Grant No. ST/L005824/1); Z.E., Z.F., and G.G. via NKFIH K120666; D.B., M.P.T., and K.S. via DFG (BE 4100/4-1) and COST (CA16117, "ChETEC").

[1] C. Abia, R. P. Hedrosa, I. Domínguez, and O. Straniero, Astron. Astrophys. **599**, A39 (2017).
[2] L. R. Nittler, C. M. O. Alexander, R. Gallino, P. Hoppe, A. N. Nguyen, F. J. Stadermann, and E. K. Zinner, Astrophys. J. **682**, 1450 (2008).
[3] S. Palmerini, M. La Cognata, S. Cristallo, and M. Busso, Astrophys. J. **729**, 3 (2011).
[4] M. Lugaro, A. I. Karakas, C. G. Bruno, M. Aliotta, L. R. Nittler, D. Bemmerer, A. Best, A. Boeltzig, C. Broggini, A. Caciolli, F. Cavanna, G. F. Ciani, P. Corvisiero, T. Davinson, R. Depalo, A. Di Leva, Z. Elekes, F. Ferraro, A. Formicola, Z. Fülöp *et al.*, Nat. Astron. **1**, 0027 (2017).
[5] C. G. Bruno, D. A. Scott, A. Formicola, M. Aliotta, T. Davinson, M. Anders, A. Best, D. Bemmerer, C. Broggini, A. Caciolli, F. Cavanna, P. Corvisiero, R. Depalo, A. Di Leva, Z. Elekes, Z. Fülöp, G. Gervino, C. J. Griffin, A. Guglielmetti, C. Gustavino *et al.*, Eur. Phys. J. A **51**, 94 (2015).
[6] C. Bruno, M. Aliotta, P. Descouvemont, A. Best, T. Davinson, D. Bemmerer, A. Boeltzig, C. Broggini, A. Caciolli, F. Cavanna, T. Chillery, G. Ciani, P. Corvisiero, R. Depalo, A. Di Leva, Z. Elekes, F. Ferraro, A. Formicola, Z. Fülöp, G. Gervino *et al.*, Phys. Lett. B **790**, 237 (2019).
[7] A. Best, F. Pantaleo, A. Boeltzig, G. Imbriani, M. Aliotta, J. Balibrea-Correa, D. Bemmerer, C. Broggini, C. Bruno, R. Buompane, A. Caciolli, F. Cavanna, T. Chillery, G. Ciani, P. Corvisiero, L. Csedreki, T. Davinson, R. deBoer, R. Depalo, A. Di Leva *et al.*, Phys. Lett. B **797**, 134900 (2019).
[8] D. Tilley, H. Weller, C. Cheves, and R. Chasteler, Nucl. Phys. A **595**, 1 (1995).
[9] M. Q. Buckner, C. Iliadis, J. M. Cesaratto, C. Howard, T. B. Clegg, A. E. Champagne, and S. Daigle, Phys. Rev. C **86**, 065804 (2012).
[10] H. T. Fortune, Phys. Rev. C **88**, 015801 (2013).
[11] A. Boeltzig, A. Best, G. Imbriani, M. Junker, M. Aliotta, D. Bemmerer, C. Broggini, C. G. Bruno, R. Buompane, A. Caciolli, F. Cavanna, T. Chillery, G. F. Ciani, P. Corvisiero, L. Csedreki, T. Davinson, R. J. deBoer, R. Depalo, A. D. Leva, Z. Elekes *et al.*, J. Phys. G: Nucl. Part. Phys. **45**, 025203 (2018).
[12] A. Formicola, G. Imbriani, M. Junker, D. Bemmerer, R. Bonetti, C. Broggini, C. Casella, P. Corvisiero, H. Costantini, G. Gervino, C. Gustavino, A. Lemut, P. Prati, V. Roca, C. Rolfs, M. Romano, D. Schürmann, F. Strieder, F. Terrasi, H.-P. Trautvetter *et al.*, Nucl. Instrum. Methods Phys. Res., Sect. A **507**, 609 (2003).

[13] C. Casella, H. Costantini, A. Lemut, B. Limata, D. Bemmerer, R. Bonetti, C. Broggini, L. Campajola, P. Cocconi, P. Corvisiero, J. Cruz, A. D'Onofrio, A. Formicola, Z. Fülöp, G. Gervino, L. Gialanella, A. Guglielmetti, C. Gustavino, G. Gyurky, A. Loiano *et al.*, Nucl. Instrum. Methods Phys. Res., Sect. A **489**, 160 (2002).
[14] H. Costantini, A. Formicola, G. Imbriani, M. Junker, C. Rolfs, and F. Strieder, Rep. Prog. Phys. **72**, 086301 (2009).
[15] D. Bemmerer, F. Confortola, A. Lemut, R. Bonetti, C. Broggini, P. Corvisiero, H. Costantini, J. Cruz, A. Formicola, Z. Fülöp, G. Gervino, A. Guglielmetti, C. Gustavino, G. Gyürky, G. Imbriani, A. P. Jesus, M. Junker, B. Limata, R. Menegazzo, P. Prati *et al.*, Eur. Phys. J. A **24**, 313 (2005).
[16] G. Gilmore, *Practical Gamma-ray Spectrometry*, 2nd ed. (Wiley, New York, 2008)
[17] LUNA Collaboration, A. Caciolli, D. A. Scott, A. Di Leva, A. Formicola, M. Aliotta, M. Anders, A. Bellini, D. Bemmerer, C. Broggini, M. Campeggio, P. Corvisiero, R. Depalo, Z. Elekes, Z. Fülöp, G. Gervino, A. Guglielmetti, C. Gustavino, G. Gyürky, G. Imbriani *et al.*, Eur. Phys. J. A **48**, 144 (2012).
[18] D. Vermilyea, Acta Metall. **1**, 282 (1953).
[19] C. Iliadis, *Nuclear Physics of Stars*, 1st ed. (Wiley-VCH, Weinheim, 2007).
[20] K. Debertin and R. G. Helmer, *Gamma- and X-ray Spectrometry with Semiconductor Detectors* (North-Holland, Amsterdam, 1988).
[21] S. J. Gelsema, Advanced γ-ray spectrometry dealing with coincidence and attenuation effects, Ph.D. thesis, Interfaculty Reactor Institute, Delft University of Technology, 2001 (unpublished).
[22] M. Blaauw and S. J. Gelsema, Nucl. Instrum. Methods Phys. Res., Sect. A **505**, 311 (2003).
[23] G. F. Knoll, *Radiation Detection and Measurement*, 3rd ed. (Wiley, New York, 2000).
[24] G. Imbriani, H. Costantini, A. Formicola, A. Vomiero, C. Angulo, D. Bemmerer, R. Bonetti, C. Broggini, F. Confortola, P. Corvisiero, J. Cruz, P. Descouvemont, Z. Fülöp, G. Gervino, A. Guglielmetti, C. Gustavino, G. Gyürky, A. P. Jesus, M. Junker, J. N. Klug *et al.*, Eur. Phys. J. A **25**, 455 (2005).
[25] J. Allison, K. Amako, J. Apostolakis, H. Araujo, P. Arce Dubois, M. Asai, G. Barrand, R. Capra, S. Chauvie, R. Chytracek, G. Cirrone, G. Cooperman, G. Cosmo, G. Cuttone, G. Daquino, M. Donszelmann, M. Dressel, G. Folger, F. Foppiano, J. Generowicz *et al.*, IEEE Trans. Nucl. Sci. **53**, 270 (2006).
[26] S. Croft, Nucl. Instrum. Methods Phys. Res., Sect. A **307**, 353 (1991).
[27] K. Spyrou, C. Chronidou, S. Harissopulos, S. Kossionides, T. Paradellis, C. Rolfs, W. Schulte, and L. Borucki, Eur. Phys. J. A **7**, 79 (2000).
[28] M. Wiescher, H. Becker, J. Görres, K.-U. Kettner, H. Trautvetter, W. Kieser, C. Rolfs, R. Azuma, K. Jackson, and J. Hammer, Nucl. Phys. A **349**, 165 (1980).
[29] M. Wang, G. Audi, A. Wapstra, F. Kondev, M. MacCormick, X. Xu, and B. Pfeiffer, Chin. Phys. C **36**, 1603 (2012).
[30] D. W. O. Rogers, R. P. Beukens, and W. T. Diamond, Can. J. Phys. **50**, 2428 (1972).
[31] S. Wilmes, V. Wilmes, G. Staudt, P. Mohr, and J. W. Hammer, Phys. Rev. C **66**, 065802 (2002).
[32] J. Dermigny, C. Iliadis, M. Buckner, and K. Kelly, Nucl. Instrum. Methods Phys. Res., Sect. A **830**, 427 (2016).
[33] R. B. Vogelaar, T. R. Wang, S. E. Kellogg, and R. W. Kavanagh, Phys. Rev. C **42**, 753 (1990).
[34] C. Iliadis, R. Longland, A. Champagne, A. Coc, and R. Fitzgerald, Nucl. Phys. A **841**, 31 (2010).
[35] C. D. Nesaraja, N. Shu, D. W. Bardayan, J. C. Blackmon, Y. S. Chen, R. L. Kozub, and M. S. Smith, Phys. Rev. C **75**, 055809 (2007).
[36] A. Di Leva, G. Imbriani, R. Buompane, L. Gialanella, A. Best, S. Cristallo, M. De Cesare, A. D'Onofrio, J. G. Duarte, L. R. Gasques, L. Morales-Gallegos, A. Pezzella, G. Porzio, D. Rapagnani, V. Roca, M. Romoli, D. Schürmann, O. Straniero, and F. Terrasi (ERNA Collaboration), Phys. Rev. C **95**, 045803 (2017).
[37] A. Boeltzig, A. Best, F. Pantaleo, G. Imbriani, M. Junker, M. Aliotta, J. Balibrea-Correa, D. Bemmerer, C. Broggini, C. Bruno, R. Buompane, A. Caciolli, F. Cavanna, T. Chillery, G. Ciani, P. Corvisiero, L. Csedreki, T. Davinson, R. deBoer, R. Depalo *et al.*, Phys. Lett. B **795**, 122 (2019).
[38] B. Povh and D. F. Hebbard, Phys. Rev. **115**, 608 (1959).
[39] H. W. Becker, W. E. Kieser, C. Rolfs, H. P. Trautvetter, and Wiescher, Z. Phys. A **305**, 319 (1982).
[40] J. F. Ziegler and J. P. Biersack, SRIM 2013, http://srim.org.
[41] C. Angulo, M. Arnould, M. Rayet, P. Descouvemont, D. Baye, C. Leclercq-Willain, A. Coc, S. Barhoumi, P. Aguer, C. Rolfs, R. Kunz, J. W. Hammer, A. Mayer, T. Paradellis, S. Kossionides, C. Chronidou, K. Spyrou, S. degl'Innocenti, G. Fiorentini, B. Ricci *et al.*, Nucl. Phys. A **656**, 3 (1999).
[42] S. Cristallo, A. Di Leva, G. Imbriani, L. Piersanti, C. Abia, L. Gialanella, and O. Straniero, Astron. Astrophys, **570**, A46 (2014).